Localization and delocalization in solids from electron distribution functions

A. Gallo-Bueno,[†] M. Kohout,[‡] E. Francisco,[¶] and Á. Martín Pendás[*,¶]

†*Center for Cooperative Research on Alternative Energies (CIC energiGUNE), Basque Research and Technology Alliance (BRTA), Álava Technology Park, Albert Einstein 48, 01510 Vitoria-Gasteiz, Spain*

‡*Max Planck Institute for Chemical Physics of Solids, Nöthnitzer Strasse 40, 01187 Dresden, Germany*

¶*Departamento de Química Física y Analítica, Facultad de Química, Universidad de Oviedo, 33006 Oviedo, Spain*

E-mail: ampendas@uniovi.es

Phone: +34 985 103037

The extent of electron localization and delocalization in molecular and condensed phases has been the subject of intense scrutiny over the years. In Chemistry, where real, instead of momentum space viewpoints are many times closer to intuition, a plethora of localization descriptors exist, including a family of indices invariant under orbital transformations that rely only on an underlying partition of the physical space into meaningful regions. These localization and delocalization indices measure the fluctuation of the electron population contained in such domains, and have been rigorously related to the insulating or conductive character of extended systems. Knowledge of the full electron population probability distribution function is also available in molecules, where it has provided many meaningful results as well as uncovered exotic interaction regimes in excited states. Electron distribution functions (EDFs), that can be seen as real

space analogs of Pauling resonance structures, are now reported in periodic systems. In agreement with what is known in finite systems, ionic compounds display narrow EDFs that get wider as covalency sets in. Contrarily to conventional wisdom, most electrons delocalize over their nearest neighbours, even in quasi electron-gas metals like sodium, and it is only in the decay rate of the probability distribution where conductors and insulators can be distinguished.

Introduction

The many years of efforts devoted to unveil the physical laws behind the behaviour of electrons in normal matter, which lie at the very root of the science of Chemistry, have been enormously influenced by a relatively small number of extraordinary scientists that cast the language that is still spoken today. Among these we find Gilbert N. Lewis,[1] whose electron-pair paved the way to the modern theory of the chemical bond, and Linus Pauling,[2] who fused the electron pair of Lewis and the Heitler-London[3] method to develop valence bond (VB) theory and to introduce, among many others, the concept of resonance, used for decades to rationalize the distribution of the electrons in molecules.

With the advent of electronic computers and their exceptional ability to tackle with linear algebra problems, valence bond theory yielded to the molecular orbital (MO) machinery,[4] and with it the theory of chemical bonding was recast into its one-electron formalism. Although we assist to a renaissance of VB theory thanks to faster and faster computers and new methodological advances,[5] both the VB and MO frameworks are built in Hilbert space, and not in the physical space of chemical intuition. This situation has led to the development of a complementary pathway independent of the orbital concept (i.e. invariant under orbital transformations) that takes the wavefunction itself in position (or momentum) space as the basic object of scrutiny. Given that not always (actually very rarely) we need the full N-electron information contained in Ψ, these real space techniques tend to compress that information by using n-particle densities, or density matrices with $n \leq N$, the so-called n-th order reduced density matrices (nRDMs). The analysis of the simplest of these, the one-particle electron density, $\rho(\boldsymbol{r})$, led to the quantum theory of atoms

in molecules (QTAIM),[6] in which an atomic partition of the physical space is provided by the attraction basins of the $\nabla\rho(\boldsymbol{r})$ vector field. This topological approach has been applied to a number of scalar fields, in what we know as quantum chemical topology.[7]

An essential feature of topological approaches is their versatility. They can be equally applied to any formalism from which RDMs can be obtained, and are thus very useful for comparison purposes. Moreover, they provide two modes of operation: the local and the global viewpoints. In the former, distinguished points in space, typically the critical points of the field being used, are related to chemical objects like bonds, lone pairs, cores, etc, and the values of a large number of magnitudes correlated to chemical behaviour. In the latter, the expectation value of each quantum mechanical observable is partitioned into a sum of domain (in the case of one-electron operators) or intra- and interdomain contributions (in the two-electron case). In the QTAIM, since the interatomic separation surface has zero local flux of $\nabla\rho$, $\nabla\rho\cdot\boldsymbol{n}dS=0$ with $\boldsymbol{n}$ being the normal vector to the surface at each point, the domain (atomic) kinetic energy is well defined for the whole family of Laplacian kinetic energy densities.[8] The QTAIM energy decomposition is in this sense rather well physically defined. Topological approaches induce exhaustive partitions of the real space that can be envisaged as a coarse–grained mapping of the electron distribution.

The topological method has provided a large number of important insights in the last decades, justifying for instance the extremely successful valence shell electron pair repulsion (VSEPR) model of the late Ronald Gillesspie,[9] or having been adopted as a paradigm by the X-ray crystallography community thanks to the measurable character of ρ. However, its new language and the lack of immediate correspondence with either the VB or MO methods have worked against its spread in other realms. It is in this sense that efforts to connect it to mainstream thinking should be welcome.

As Pauling's resonance is regarded, a real space analog has already been proposed in isolated molecules through the so-called electron distribution functions (EDFs),[10] which provide the statistical distribution of the N electrons of a molecule into its m atomic basins. A real space resonant structure (RSRS) is regarded as one of the possible $(N+m-1)!/\{N!(m-1)!\}$ partitions. The EDF formalism allows us to compute the probability of finding each of these electron distributions. It also provides a very convenient picture

in which an atom contains a fluctuating number of electrons, i.e. in which an atom is an open quantum system (OQS) within a molecule.[11] The consideration of an atom as an OQS also allows to compute the contribution of each of its resonance structures to its local spin[12] or to any other observable.

EDFs have been successfully used to recast Pauling's concepts in an orbital invariant manner,[10,13,14] but, so far, have only been available in finite systems. In this paper we extend the EDF concept to crystalline solids. We first introduce briefly the EDF framework, paying attention to how the statistical moments of the EDF can be used to access fluctuation-like concepts like electron localization and delocalization indices, which constitute the real space analogs of bond orders. The extension of the formalism to periodic systems follows, and we end by showing results in a set of four paradigmatic systems that have been used in similar circumstances in the past:[15] metallic Na in its *bcc* phase, NaCl, diamond and graphite. Application to other chemically or physically interesting systems is straightforward and under way, but out of the scope of this methodological introduction.

As it will become clear, the EDF formalism depends only on a pre-selected partition of space. This implies that, after this work, EDFs are available not only for atomic partitions like the one here explored, but for a plethora of other possibilities, including electron-pair partitionings like those offered, for instance, by the electron localization function (ELF) of Becke and Edgecombe[16] or the Electron Localizability Indicator (ELI).[17] Since fluctuations of the electron population of electron pair regions are interpreted rather differently than those of atomic-like domains, only the latter are explored here.

Methodology

Electron distribution functions and real space resonance structures

Let us introduce an atomic partition of the physical space (like that provided by the QTAIM, although many other options are available in the literature) and count how many electrons are found in each of the m different atomic regions of the system. In the large numbers limit, this information can be condensed into the joint probability distribution of finding a given partition $S = (n_1, n_2, \ldots, n_m)$ of the electrons into the

m atomic domains, whereby $\sum_{i=1}^{m} n_i = N$ is the total number of electrons. The partition S is termed a real space resonance structure (RSRS) and collected into the electron distribution function (EDF) of the system. If the latter is described by a wavefunction $\Psi(1,\ldots,N)$, then the probability $p(S)$ of partition S is given by[18]

$$p(S) = \mathcal{P} \int_D \Psi^* \Psi d\boldsymbol{x}_1 \boldsymbol{x}_2 \cdots d\boldsymbol{x}_N, \tag{1}$$

where electron i is described by its $\boldsymbol{x}_i$ spin-spatial coordinate, the combinatorial factor prior to the integral, $\mathcal{P} = N!/(n_1! \ldots n_m!)$, takes into account indistinguishability, and D is a real space domain in which the first n_1 electrons are integrated over atomic region number one, the second n_2 electrons over atomic region two, etc. If the spin coordinates are not integrated, this is the spin-resolved partitition,[19] in which we specify also the m_s value of each electron and $S \equiv \{n_1^\alpha, n_2^\alpha, \ldots, n_m^\alpha; n_1^\beta, n_2^\beta, \ldots, n_m^\beta\}$.

In the last years, algorithms to calculate EDFs in finite systems for both single-determinant and explicitly correlated wavefunctions have been devised.[18] In the density functional theory (DFT) context, that overhwhelms the literature for periodic systems, it has been customary to build Fock-Dirac-like density matrices from the Kohn-Sham determinant,[20] although these do not provide true nRDMs. If $\Psi(1,\ldots,N) = (N!)^{-1/2}\det\ |\chi_1(1)\ldots\chi_N(N)|$, where χ_1, $\ldots$, χ_N are the N occupied orbitals, then the probability of a partition S is given by (see Ref. 18 and reference therein)

$$p(S) = \mathcal{N} \sum_{\{k_j\}\in\mathcal{S}_N} \det\left[S_{ij}^{b(k_j)}\right], \tag{2}$$

where $\mathcal{N} = \mathcal{P}/N!$, $\mathcal{S}_N$ is the set of $N!$ permutations of the $1\ldots N$ set and $\{k_j\} \equiv \{k_1,\ldots,k_N\}$ is one of these permutations. The overlap integrals $S_{ij}^{b(k_j)}$ between the orbitals χ_i and χ_j are projected over the atoms in the order that leads to the partition S subjected to permutation k_j. If we choose a real space atomic partitioning, then

$$S_{ij}^{b(k_j)} = \int_{\Omega_b} \chi_i(\boldsymbol{x})\chi_j(\boldsymbol{x})d\boldsymbol{x}, \tag{3}$$

where we integrate over the atomic domain of atom b, Ω_b. Notice that the above expression for $p(S)$

involves a combinatorial explosion of terms as the system's size grows, making it unusable except in the very simplest cases.

We have already shown[18] that, after some algebraic rearrangements, we can obtain $p(S)$ simultaneously for all S's as the solution of the linear system,

$$\sum_S t_1^{n_1} t_2^{n_2} \dots t_m^{n_m} p(S) = \det \left[\sum_{k=1}^{m} t_k S^k \right], \tag{4}$$

where the t_k are arbitrary real numbers, S^k is the atomic overlap matrix (AOM) of atom k, and the sum in the left-hand side only includes the $S \equiv \{n_p\}$ sets with $n_1 + n_2 + \dots + n_m = N$. This system is solved with the same strategies already described,[13,14,18] with the set of basin restricted overlap integrals as the only necessary object between all pairs of orbitals in the wavefunction expansion. Although the size of the linear system may be very large, this technique allows to by-pass the above-mentioned combinatorial explosion.

The number of RSRSs grows rapidly with the number of electrons and nuclei. For instance, it equals 4 in H_2, 66 in H_2O, or 286 in NH_3, but climbs to 76 223 753 060 in benzene.[10] Fortunately, as it is done in conventional VB calculations, we can substantially reduce this number by grouping non-relevant functional groups together, for instance, leaving only the chemically active components. Similarly, one can impose restrictions that limit the size of the EDF vector of probabilities. In benzene, the probability of finding all the 42 electrons in the region associated to a given C or H atom is negligible, and can be discarded from the start. Chemically sensible approximations can also be done, like associating all core electrons directly to their appropriate atomic basins without delocalization to other spatial regions.

Localization and Delocalization from EDF statistics

The computation of the EDF provides all kind of statistical measures. Since the full joint probability distribution has been obtained, we can easily build marginals from it. For instance, the one-atom distribution $p(n_1)$ provides the probability of finding a given number of electrons in atom 1, $p(n_1) = \sum_{n_2,\dots,n_m} p(n_1, n_2, \dots, n_m)$. This tells us how much the atomic population entangles with the rest of the system. Its Shannon entropy

$\sum_i p(i)\log_2(p(i))$ does only vanish if the atom is isolated. Moreover, the first moment of this one-atom distribution, $\langle n_1\rangle = \sum_i i \times p(i)$ gives the standard atomic electron population, which can also be written as $\int_{\Omega_1} \rho(\boldsymbol{r})d\boldsymbol{r}$. Two-, and in general, n-atom marginals contain relevant information about population fluctuations or, in chemical terms, about bonding, be it two- or multicenter in nature. This information is gathered through the several central or cumulant moments of the distributions.[21] Provided that there is only a finite number of marginal distributions, we can take advantage of this with taxonomic purposes. For instance, if we are interested in two-electron, two-center bonding, there are only three different electron partitions for such a system: either the two electrons lie in the first atom, one in the first and the other in the second, or the two electrons are found in the second atom. Since the sum of the probabilities of these three events add to one, all 2c,2e electron distributions depend on two independent parameters. A statistical classification of 2c,2e bonds is thus available.[10,22] These ideas can be easily generalized.[21]

The next simplest moments that can be envisioned are the one-center variance and the two-center covariance of the atomic populations:

$$\mathrm{var}(n_A) = \sum_{n_A} p(n_A)(n_A - \langle n_A\rangle)^2,$$

$$\mathrm{cov}(n_A, n_B) = \tag{5}$$

$$\sum_{n_A,n_B} p(n_A, n_B)(n_A - \langle n_A\rangle)(n_B - \langle n_B\rangle). \tag{6}$$

These provide a direct, orbital invariant measure of the spread of their electron distribution. A zero variance region implies a perfect spatial electron localization, with a one-center probability that does only contain one component: $p(n_A) = 0\ \forall n_A \neq \langle n_A\rangle$. As the width of $p(n_A)$ increases and the electrons delocalize over other atomic regions, the latter can be recognized by the A, B covariance, which determines the correlation between both electron populations. Obviously $\sum_A \mathrm{var}(n_A) + \sum_{A,B} \mathrm{cov}(n_A, n_B) = 0$.

Thus, it is fruitful to build a set of descriptors related to the degree of electron localization and delocalization from the above moments. These are called the (atomic) localization index (LI) $\lambda^A = \langle n_A\rangle - \mathrm{var}(n_A)$ and the (interatomic) delocalization index (DI) $\delta^{A,B} = -2\,\mathrm{cov}(n_A, n_B)$, respectively.[23,24] Since they are

subjected to the sum rule

$$\lambda^A + \frac{1}{2}\sum_{B\neq A}\delta^{A,B} = \langle n_A \rangle, \tag{7}$$

they can be loosely identified with the number of localized electrons λ^A in the region A and the number of delocalized electrons $\delta^{A,B}$ between two regions.

The DI is the real space equivalent of the Wiberg-Mayer (WM) bond order,[25,26] and has been widely used. We have shown[22] how to rationalize this equivalence from statistical grounds. An ideal 2c,2e bond, for instance, is that in which the two electrons delocalize freely over the two atoms. This leads immediately to a binomial distribution, where the joint probability of finding the two electrons in one of the atoms, $p(2,0) = p(0,2) = 1/4$, and $p(1,1) = 1/2$. It is immediately found that the covariance of this distribution leads to $\delta^{A,B} = 1$. Similarly, when two independent ideal electron pairs exist (like, in an approximate way, in the double σ, π link in ethylene) the additivity of covariances for independent events leads to $\delta^{A,B} = 2$. It should be noticed that there are in principle many possible EDFs leading to the same LIs and DIs, so that the availability of the former provides a much thinner description of localization and delocalization than that provided by the latter.

The DI machinery has already been generalized to periodic systems,[15,27,28] paving the way to a better understanding of how electrons localize and delocalize in solids. After the developments shown below, the much more fine-grained EDF description enlarges the toolkits available to understand the electronic structure of solids.

Electron distribution functions in the solid state

Let us then focus on a typical single determinant approximation to the wavefunction of a solid, coming either from a periodic Hartree-Fock calculation, or from a Kohn-Sham determinant in the DFT case. Then, the AOMs (Eq. 3) inserted in the Eq. 2 are computed for the occupied Bloch states $\psi_{n,\boldsymbol{k}}$ labeled with the band n and $\boldsymbol{k}$ vector indices and feed the algorithm described in Eq. 4, which has been implemented in the

EDF code by Francisco and co-workers[13,14]

$$S_{n\boldsymbol{k},n'\boldsymbol{k}'}(\Omega) = \int_{\Omega} \psi^{\star}_{n,\boldsymbol{k}}(\boldsymbol{r})\psi_{n',\boldsymbol{k}'}(\boldsymbol{r})\, d\boldsymbol{r}. \tag{8}$$

If this approach is used then the delocalization index between regions A and B becomes

$$\delta^{A,B} = \frac{2}{K^2_{BZ}} \sum_{n,n'} \sum_{\boldsymbol{k},\boldsymbol{k}'} S_{n\boldsymbol{k},n'\boldsymbol{k}'}(A) S_{n\boldsymbol{k},n'\boldsymbol{k}'}(B) \theta(n,\boldsymbol{k})\theta(n',\boldsymbol{k}'), \tag{9}$$

where the occupation number function $\theta(n,\boldsymbol{k})$ selects the corresponding occupied states, allowing for a convenient smearing of the Fermi surface states in the case of metals, and K_{BZ} is the total number of $\boldsymbol{k}$ points used in the calculation.

Computational details

In order to get results comparable to those previously obtained in the work by A. Baranov and M. Kohout,[15] we have obtained the EDFs of the same systems studied there: NaCl as a model of ionic bonding, diamond and graphite as covalent prototypes, and Na in its *bcc* phase as paradigm of metallic behaviour. All those systems were described within a DFT framework, with wavefunctions obtained through the solid state FP-LAPW code Elk,[29] and using the local spin density approximation with the Perdew-Wang exchange-correlation functional.[30] All calculations were done using a fine logarithmic mesh, by setting the parameter `lradstp`$= 1$ in Elk. A $4 \times 4 \times 4$ $\boldsymbol{k}$-points mesh was used in all cases, except in graphite where a $4 \times 4 \times 3$ grid was selected. The mesh was shifted with `vkloff` $= (0.25, 0.5, 0.75)$ in NaCl and Na, and with $(0.25, 0.5, 0.625)$ in diamond and graphite. Additionally, a very small smearing width was used (`swidth` $\approx 10^{-8}$) in order to provide as pure occupations of the orbitals as possible, except in diamond and graphite where it was increased to 10^{-5}. In these cases, the width does not impact results and can be chosen large to speed up the process. The expansion cutoff for the wave function was set to 7.0 a.u. (parameter `rgkmax`). Default parameters were used otherwise.

Table 1 The average atomic population $\langle n_A \rangle$, the localization index λ^A and the fluctuation $2\sigma_A^2$ of atom A in the examined compounds. $\delta^{1,2}$ and $\delta^{1,3}$ refers to the DIs between the first and second neighbours. In graphite, C–$C_{\parallel}$ stands for the DI between first-neighbour carbon atoms in the same layer and C–$C_{\perp}$ between first-neighbours of different layers.

	A	$\langle n_A \rangle$	λ^A	$2\sigma_A^2$	$A-B$	$\delta^{1,2}$	$\delta^{1,3}$	$\delta^{1,4}$
NaCl	Na	10.142	9.975	0.334	Na–Cl	0.334		
molecule	Cl	17.858	17.691	0.334				
NaCl	Na	10.148	9.920	0.456	Na–Cl	0.074		
solid	Cl	17.852	17.334	1.036	Cl–Cl		0.048	
Diamond	C	5.994	3.808	4.372	C–C	0.914	0.039	
Graphite	$C_{\parallel}$	5.991	3.864	4.254	C–$C_{\parallel}$	1.211	0.055	0.039
	$C_{\perp}$	6.020	3.871	4.298	C–$C_{\perp}$	0.020	0.007	
Na *bcc*	Na	10.997	10.199	1.596	Na–Na(3.66Å)	0.096	0.003	
					Na–Na(4.22Å)	0.059		

Later on, the space was QTAIM partitioned, and all products of crystal orbitals integrated over the resulting basins to yield the AOMs needed to feed Eq. 2 by means of the DGrid code[31] (starting with DGrid-5.2 the AOMs can be evaluated also for the FHI-aims solid state program[32]). The evaluation of molecular EDFs for both single-determinant as well as for correlated wave functions is implemented in the EDF code.[14] Since crystal orbitals are complex in general, and so are the AOMs computed with DGrid, we have coded a suitable generalization of the EDF program to deal with extended systems. The solid state calculations were done with this EDF extension, available at `https://github.com/eveliofrancisco/EDF`.

Results and discussion

Crystalline NaCl: the ionic case

The NaCl diatomic molecule is a typical example of an ionic system. The high difference in electronegativity between both atoms give rise to the asymmetric electron sharing: the Cl atom increases its population,

leading to a distribution close to the canonical picture Na^+Cl^-. The LIs within the QTAIM basins are high, $\lambda^{Na} = 9.98$ and $\lambda^{Cl} = 17.69$, and very similar to the QTAIM populations $\langle n_{Na} \rangle = 10.14$ and $\langle n_{Cl} \rangle = 17.86$. Thus, the variance or fluctuation in the electronic population σ^2, obtained as the difference between the QTAIM population $\langle n_M \rangle$ and λ (see Ref. 15) can be considered to be very low $\sigma^2_{Na} = \sigma^2_{Cl} = 0.17$. High localization with values close to the basin population are in good agreement with the results obtained for the simplest prototype of ionic bond LiH,[23,33] with fluctuations of $\sigma^2_{Li} = \sigma^2_{H} = 0.10$.[33] The DI and LI values for the NaCl molecule are summarized in Table 1.

The resonance structure with highest probability in the NaCl diatomic molecule is $p^1(n_{Na} = 10) = p^1(n_{Cl} = 18) = 0.838$, leading to the expected ionic Na^+Cl^- case. In a binary compound, the loss of one electron by one of the components immediately implies its acceptance by the other with the same probability, so that the covariance between both populations is necessarily negative, and knowledge of the one domain probabilities is equivalent to the full EDF.

The above scenario is no longer true in solid NaCl, where an electron lost by a sodium moiety could in principle delocalize over a large number of other atomic regions. This means that the two-domain probabilities (p^2) could, in principle, be decoupled from one-domain probabilities (p^1). However, if the populations of two atoms where fully uncorrelated, with zero mutual covariance, then their joint probability could be calculated directly from the one-domain probabilities. This is expected to be approximately fulfilled in an ionic solid. We have gathered some one- and two-domain probabilities calculated for the NaCl crystal in Table 2.

Let us first examine the one-domain probabilities. The most probable number of electrons in sodium is 10, as expected, with $p^1(n_{Na} = 10) = 0.798$, followed by the neutral population with $p^1(n_{Na} = 11) = 0.154$. Notice that the sum of these two is around 0.95. On the contrary, the equivalent counts for the Cl atom, 18 and 17 electrons, display probabilities equal to 0.620 and 0.216, respectively. They add to about $p = 0.84$, a value considerably different from the sum in Na. Although the most likely electron counts are clearly those of the ionic situation, the Cl atom is engaged in a more extensive delocalization network than sodium, in agreement with chemical intuition: given the considerably larger polarizability and softness of the chloride

Table 2 Probabilities of different RSRSs in the NaCl crystal. p^1 and p^2 refer to one- and two-domain probabilities, respectively, indicating in parenthesis the species involved. The last column provides a measure of the deviation from the independent particle situation, in which the product of the probabilities of the events should equal the probability of the joint event, $p^2(n_{\mathrm{Na}}, n_{\mathrm{Cl}}) = p^1(n_{\mathrm{Na}}) \times p^1(n_{\mathrm{Cl}})$.

n_{Na}	n_{Cl}	$p^1(n_{\mathrm{Na}})$	$p^1(n_{\mathrm{Cl}})$	n_{Na}	n_{Cl}	$p^1(n_{\mathrm{Na}}) \times p^1(n_{\mathrm{Cl}})$	$p^2(n_{\mathrm{Na}}, n_{\mathrm{Cl}})$	$p^2 - p^1_{\mathrm{Na}} p^1_{\mathrm{Cl}}$
10	18	0.7982	0.6197	10	18	0.4946	0.5086	0.0140
11	17	0.1537	0.2155	10	17	0.1720	0.1620	-0.0100
9	19	0.0335	0.1177	10	19	0.0939	0.0943	0.0004
12	16	0.0132	0.0326	11	18	0.0952	0.0851	-0.0101
13	20	0.0007	0.0110	11	17	0.0331	0.0428	0.0097
8	15	0.0006	0.0027	10	16	0.0260	0.0223	-0.0037

anion, it accommodates much more easily a fluctuation of its electron population than the sodium cation.

It is also informative to consider the RSRSs with smaller probabilities. In Fig. 1 we present the one-domain probabilities of the RSRSs with the largest weight for all our systems. In the left diagram, the $\Delta Q_{ref} = 0$ bar corresponds to the most probable RSRS, and positive (negative) values of ΔQ_{ref} imply that the atom has gained (lost) electrons with respect to it. In the case of solid NaCl, purple and red bars stand for Na and Cl, respectively, which at $\Delta Q_{ref} = 0$ represent the most probable Na^+ and Cl^- distribution. Both atoms show a very asymmetrical distribution of their resonance structures, that differ in the width of the distribution and the shape of its tail. The more polarizable chlorine atom shows a notably wider probability tail than sodium, and if we order the $p(n_{\mathrm{Cl}})$ values by decreasing values of p, we have to run over seven n's before reaching the $p \approx 0.0001$ threshold. The latter is reached at the fifth n value in the case of the sodium moiety. Moreover, the tail in Na is heavily displaced toward positive ΔQ_{ref} values, while the opposite is true in Cl. In other words, the ordering of the RSRSs is $p(\mathrm{Na}^+) > p(\mathrm{Na}) > p(\mathrm{Na}^{2+}) > p(\mathrm{Na}^-)$. This scheme is in tune with results already discussed in the LiH molecule,[34] and has a very very clear, simple physical root. The high energetic cost of removing two electrons from a Na atom (47.286 eV) makes the $Na^{2+}Cl^{2-}$ a very energetically costly species. The Na^-Cl^+ is in turn hindered by the expensive ionization energy of chlorine (12.967 eV).

In the AB rock-salt structure the ion A is surrounded by six B nearest neighbours (nn) and twelve A next nearest neighbours (nnn). We notice that, as shown in Fig. 2, the QTAIM Na-domain displays nn

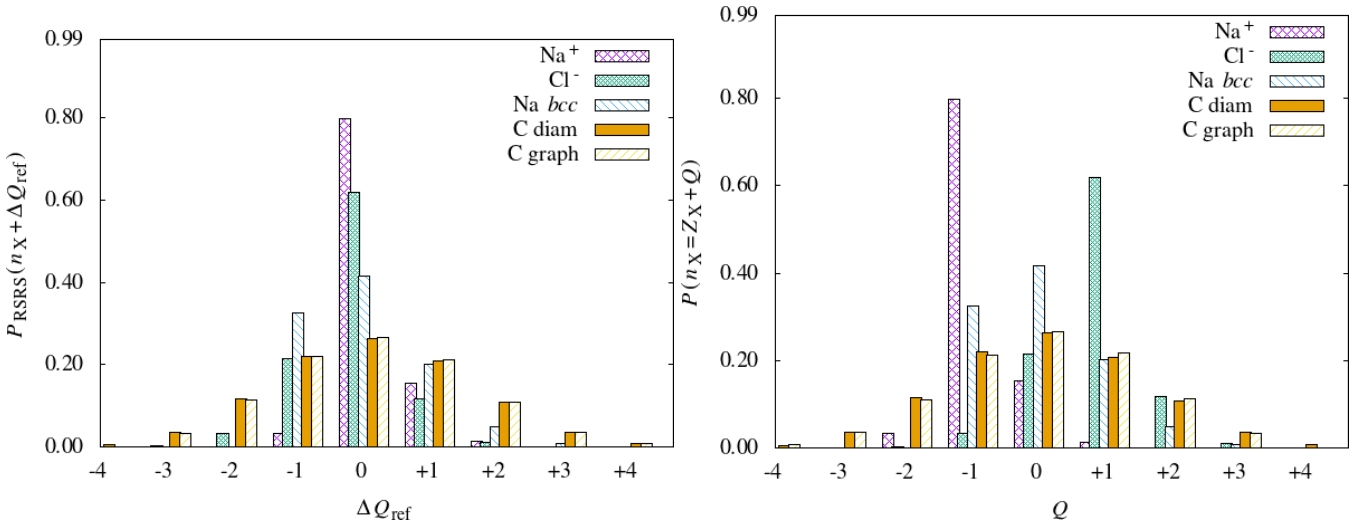

Figure 1 Bar chart representation of the largest one-centre probabilities for $X = \mathrm{Na}^+$, Cl^- (in NaCl), C in diamond and graphite, and Na *bcc*. Left: ΔQ_{ref} refers to the deviations in the number of electrons n_X of the atoms with respect to the most probable resonant structure, so that at $\Delta Q_{ref} = 0$ each atom has the electrons of the most probable RSRS. Right: Q refers to the atomic charge, and each atom at $Q = 0$ is neutral, with a probability that will be that of the atom with a number of electrons equal to its atomic number Z_X.

Na-Cl bond critical points only,[35] so that its six interatomic surfaces are the Cl contacts. On the contrary, given the considerably larger size of the chlorine domain, the Cl basin shows 6 concave Na contacts and 12 planar Cl-Cl ones. Just from this geometrical basis, which was used years ago to justify Pauling's rules from topological grounds,[36,37] the larger delocalization of Cl can be rationalized.

The total DI of a Na atom with the rest of the solid is $2\sigma^2_{\mathrm{Na}} = 0.455$, cf. Table 1, while that of a chlorine atom is considerably larger, $2\sigma^2_{\mathrm{Cl}} = 1.038$. For the Na atom, the total delocalization is almost exclusively due to the six nn-interactions yielding the close sharing[15] $\varsigma_{\mathrm{c}}^{\mathrm{Na}} = 6 \times \delta^{\mathrm{Na,Cl}} = 6 \times 0.074 = 0.444$ (the next 12 closest Na atoms plays no role in the electron sharing with the examined Na atom). The value of 0.444 is somewhat larger than the DI value $\delta^{\mathrm{Na,Cl}} = 0.334$ for the NaCl diatomic. This means that the valence capacity of a sodium atom is almost fully saturated in the molecule. This effect lies behind the well known lengthening of bond distances with increasing coordination dictated by Pauling's rules. The bonding capacity of stiff cationic species has to be shared among their neighbours. In case of the Cl atom there are additionally 12 relatively high DIs $\delta^{\mathrm{Cl,Cl}} = 0.048$ with the neighboring Cl atoms, yielding for the Cl atom the close sharing $\varsigma_{\mathrm{c}}^{\mathrm{Cl}} = 6 \times \delta^{\mathrm{Na,Cl}} + 12 \times \delta^{\mathrm{Cl,Cl}} = 6 \times 0.074 + 12 \times 0.048 = 1.02$. Thus, the

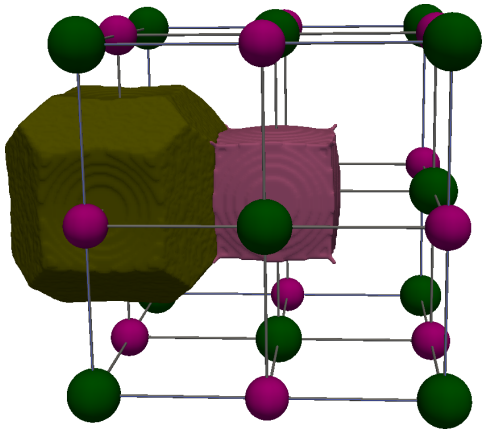

Figure 2 QTAIM basins of Na and Cl atoms in the NaCl crystal. Na atoms in magenta are smaller than the Cl atoms, in green.

close sharing is much larger for the Cl atom than for the Na counterpart. It is instructive to compare the distant sharing[15] $\varsigma_{\rm d}$ for the two atomic sorts, i.e. sharing reaching outside the close atoms. This leads to $\varsigma_{\rm d}^{\rm Na} = 2\sigma^2_{\rm Na} - \varsigma_{\rm c}^{\rm Na} = 0.455 - 0.444 = 0.011$ and $\varsigma_{\rm d}^{\rm Cl} = 2\sigma^2_{\rm Cl} - \varsigma_{\rm c}^{\rm Cl} = 1.038 - 1.02 = 0.018$, values very close to each other. This tells us about the short-range, exponentially decaying nature of electron delocalization in insulators, a subject that has been already analyzed.[38,39]

Each of the numbers that have been analyzed in the paragraph above can be dissected in much more detail once EDFs are available, since DIs and a plethora of other multicenter delocalization descriptors are, as we have summarized, nothing but appropriately built moments of the statistical distribution of electron populations[24,33,40,41] (see Eq. 5). Since the aim of this work is to present EDFs in solids, we will restrict to the nn Na-Cl interaction in Table 2. The nn Na-Cl delocalization index $\delta^{\rm Na,Cl}$ is now understood as the two-domain covariance in Eq. 5. Although the number of RSRSs contributing is larger than the once compiled in the Table 2, the data displayed suffices for the following. The joint distribution is not far from, but it is clearly different from the product of one-domain probabilities (otherwise the covariance would vanish). The last column in the Table shows the difference between p^2 and the product of independent-like p^1 events. The ionic distribution $(10, 18)$, for instance, has a positive $p^2 - p^1 p^1$ difference, while others, like the $(11, 17)$ one display a negative value. This shows how the correlation between the basin populations is built. Some joint distributions become over-represented with respect to others. It is important to recognize that there

Table 3 Probabilities of different RSRSs in diamond. C' is a nn C atom.

n_{C}	$p^1(n_{\mathrm{C}})$	n_{C}	$n_{\mathrm{C}'}$	$p^1(n_{\mathrm{C}}) \times p^1(n_{\mathrm{C}'})$	$p^2(n_{\mathrm{C}}, n_{\mathrm{C}'})$	$p^2 - p^1_{\mathrm{C}} p^1_{\mathrm{C}'}$
6	0.2640	6	6	0.0697	0.0708	0.0011
5	0.2200	5	6	0.0581	0.0587	0.0005
7	0.2078	6	7	0.0549	0.0556	0.0006
4	0.1158	5	7	0.0457	0.0507	0.0050
8	0.1079	5	5	0.0484	0.0437	-0.0047
9	0.0363	7	7	0.0432	0.0392	-0.0040
3	0.0349	4	6	0.0306	0.0302	-0.0004

are infinitely many electron distributions compatible with a given DI.[22] This means that the EDF contains far more chemical information than standard delocalization measures. For instance, one can readily check that over-expressed resonance structures tend to be Na-Cl electron conserving, i.e. $n_{\mathrm{Na}} + n_{\mathrm{Cl}} = 28$. These structures thus maintain the electroneutrality of the Na-Cl group, a result that is easily interpreted from the chemical point of view. The generality of this and other findings remains to be studied.

The large ionicity in NaCl implies that it is better to measure population fluctuations with respect to the ionic Na^+ and Cl^- charged species and not the neutral populations. This reference provides the smallest variance possible if an integer number of electrons is assumed. For instance, taking the standard variance measured with respect to the mean, $n_{\mathrm{Na}} - \lambda^{\mathrm{Na}} = 0.228$.

Diamond and graphite: the covalent cases

Crystalline carbon provides us with two extensively studied covalently bonded networks where the impact of electron delocalization on the width and global structure of the EDF can be easily studied: the diamond and graphite structures. Their computed QTAIM basins are found in Figs. 3 and 4, respectively.

In diamond, see Table 3, in contrast to what is found in NaCl the carbon atom displays a one-domain distribution which is centered at its neutral population of six electrons, extending almost symmetrically to the left and to the right of this number. Fig. 1 shows that there exists a non-negligible probability of finding from two to ten electrons in the carbon basin, and that the width of the distribution is the largest among all the ones studied here. In agreement with previous works,[18,19] this distribution is compatible with

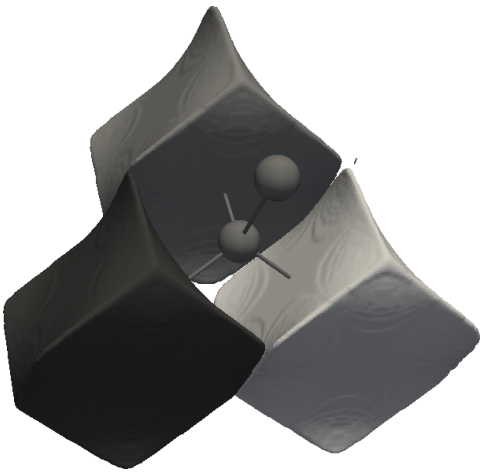

Figure 3 QTAIM basins in diamond.

multinomial statistics. In chemical terms, each of the four equivalent C-C bonds is able to provide or extract an electron of its Lewis pair, so that each C atom may display from $Z-4$ to $Z+4$ electrons.

If no further delocalization is allowed beyond that of a carbon and its tetrahedral network, then the simple multinomial model corresponds to a quadruple two-center, two-electron (2c,2e) ideal bond between the C and its tetrahedral environment. We have repeatedly shown[21] that such a 2e link provides a binomial distribution in which the $(0,2),(1,1)$, and $(2,0)$ structures have probabilities of $1/4, 1/2, 1/4$, respectively. The quadruple direct product of this binomial set yields in carbon (with a reference population of six electrons) $p(6 \pm n) = \binom{8}{4-n}/2^8$, which gives $p(6) = 0.273$, $p(5) = p(7) = 0.219$, $p(4) = p(8) = 0.109$, $p(3) = p(9) = 0.031$, and $p(2) = p(10) = 0.004$. It is surprising how such simple electron counting arguments are reproduced by actual calculations. Notice that the variance of a set of independent events is additive, and that for such an atom engaged in an ideal 2c,2e bond (the variance of the binomial set above) is equal to $1/2$. This leads to a value equal to 2 for four independent 2c,2e ideal links. Our data show that for diamond var(C) $= \langle n_{\mathrm{C}} \rangle - \lambda^{\mathrm{C}} = 2.186$, relatively close to 2. This means that only about 0.2 units out of the total variance of the C atom population is due to anything outside its tetrahedral arrangement of first neighbor bonds, pointing to small long-range delocalization.

Two-domain joint probabilities allow us to reconstruct the C-C delocalization indices. As shown in Table 1, the nn distribution yields a value close to that expected for a single bond, $\delta^{\mathrm{C,C'}} = 0.914$, which can

be compared to the the equivalent $\delta^{1,2} = 0.988$ computed in the analogous C–C single bond in C_2H_6.[33]

Table 4 1- (p^1) and 2- (p^2) domain probabilities between nearest neighbour C atoms in the same layer ($p^2_{\parallel}$) and between layers ($p^2_{\perp}$) of graphite.

n_{C}	$p^1(n_{\mathrm{C}})$	n_{C}	$n_{\mathrm{C}'}$	$p^1(n_{\mathrm{C}}) \times p^1(n_{\mathrm{C}'})$	$p^2_{\parallel}(n_{\mathrm{C}}, n_{\mathrm{C}'})$	$p^2_{\perp}(n_{\mathrm{C}}, n_{\mathrm{C}'})$	$p^2_{\parallel} - p^1_{\mathrm{C}} p^1_{\mathrm{C}'}$	$p^2_{\perp} - p^1_{\mathrm{C}} p^1_{\mathrm{C}'}$
6	0.2666	6	6	0.0711	0.0734	0.0708	0.0029	0.0003
5	0.2187	5	6	0.0583	0.0592	0.0587	0.0019	0.0004
7	0.2116	6	7	0.0564	0.0576	0.0565	0.0009	0.0001
4	0.1128	5	7	0.0463	0.0532	0.0469	0.0074	0.0006
8	0.1094	5	5	0.0478	0.0414	0.0479	-0.0055	0.0001
9	0.0358	7	7	0.0448	0.0392	0.0444	-0.0065	-0.0004
3	0.0332	4	7	0.0239	0.0299	0.0244	0.0065	0.0005
10	0.0070	5	8	0.0239	0.0302	0.0244	0.0063	0.0005

Graphite provides another interesting example, for the traditional viewpoint assigns an aromatic-like intra-layer bonding network of sp^2 bonded carbons with much weaker dispersion enhanced inter-layer interactions. Carbon atoms occupy two Wyckoff positions $(2b, 2c)$, and display two types of bond critical points: one links the $2b, 2c$ atoms (the intra-layer or parallel bond) and the other links atoms of the same sublattice belonging to neighbouring layers (the inter-layer or perpendicular bond, Fig. 4). Aromatic systems have been fully studied from several real space viewpoints.[41–43] In graphite, we have found $\delta^{\mathrm{C},\mathrm{C}'}_{\parallel} = 1.211$ with $\mathrm{var}(C)_{\text{graphite}} = 2.127$. As it is expected,[38] the DI drops one order of magnitude when considering second neighbors or the *meta*-DI, $\delta^{1,3}_{graph,\parallel} = 0.055$, but is of similar magnitude as the $\delta^{1,4}_{graph,\parallel} = 0.039$ or *para*-DI. The inter-layer delocalization $\delta^{\mathrm{C},\mathrm{C}'}_{\perp} = 0.020$ is much smaller. These values are again in very good agreement with ideal models of aromatic bonding, e.g the ideal DI between nearest neighbour carbon atoms in benzene is equal to $1 + 4/9 \approx 1.44$, and show that the inter-layer interaction is of a fundamentally different nature than the intra-layer one. Notice that much can be written about these results, which anticipate the future power of our approach. For instance, in a tight-binding (or Hückel) description of benzene and other alternate conjugate hydrocarbons it can be readily shown,[38,39] that the *meta*-like delocalization indices vanish, while the *para*-like ones do not. This is a result of quantum mechanical interference which is progressively destroyed as electron correlation sets in, as modeled by, for instance, a Hubbard Hamiltonian. The fact that the *para* delocalization index in graphite is larger than the one expected for its associated C-C

distance given an exponential decay law, as well as the non-zero, but small, value of the *meta* delocalization, are providing interesting clues about how the extended network and the interlayer contacts in graphite affect the overall delocalization pattern.

Just to summarize, in their 2011 analysis, Baranov and Kohout[15] provided electron-pair sharing values of 83% with the first neighbourhood, 11% with the second and 6% with the rest of the solid in diamond. Graphite leads to an almost identical relative distant sharing, with 15% of the shared pairs being delocalized within the second and farther distant neighbour shells. Relevant EDF descriptors for graphite are found in Table 4. At first sight, no striking differences in the probabilities themselves can be observed for the intra- and inter-layer interactions. Actually, both the one- and two-domain probabilities are rather similar to those in diamond. This shows how transferable probabilities can be in similar environments, a fact that has already been reported.[44] However, upon a closer inspection, Table 4 reveals that the two-domain inter-layer probabilities are extremely close to the product of the appropriate one-basin events. In other words, the electron populations of atoms belonging to different layers are basically decoupled, or statistically independent, and their interaction is very weak. This also stems from the difference between the intra- and interlayer δ's, 1.211 versus 0.020 au.

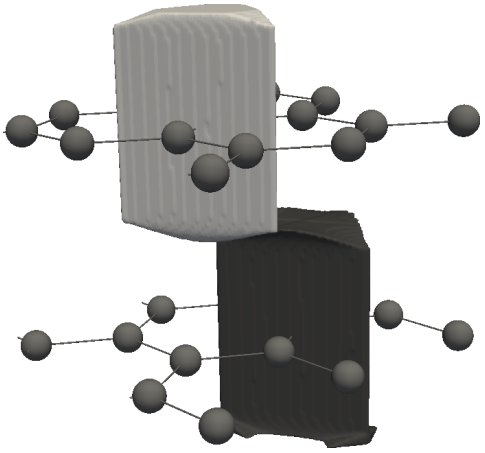

Figure 4 Graphite QTAIM basins in different layers.

Being statistical data, we can subject probabilities to many insightful manipulations. For instance, in Table 5, we add up all the two-domain A, B probabilities that conserve the number of electrons, $n_A + n_B =$

Table 5 Probabilities of the one-domain A, B superbasin containing a given number of electrons given by $n = Z_A + Z_B$ and $n \pm 1, n \pm 2$ in the systems under scrutiny.

	$A-B$		$p(n = Z_A + Z_B)$	–1	+1	–2	+2
NaCl	nn:	Na-Cl	0.5594	0.1848	0.1894	0.0303	0.0290
	nnn:	Na-Na	0.6473	0.2464	0.0537	0.0448	0.0021
	nnn:	Cl-Cl	0.4472	0.1464	0.2749	0.0253	0.0844
diamond	nn:	C-C	0.2118	0.1821	0.1864	0.1188	0.1239
	nnn :		0.1891	0.1669	0.1711	0.1190	0.1225
graphite	nn:	$(\text{C-C})_{\parallel}$	0.2241	0.1918	0.1923	0.1206	0.1198
		$(\text{C-C})_{\perp}$	0.1905	0.1690	0.1722	0.1200	0.1233
Na *bcc*	nn:	Na-Na	0.3149	0.2052	0.0639	0.2698	0.0973
	nnn :		0.3011	0.2179	0.2439	0.1038	0.0872

n, and compare them across systems. The $p(n = Z_A + Z_B)$ column displays the probability that the two basins exchange electrons between themselves, and the rest the likeliness that an external transfer takes place. First, it should be clear that these superbasins, containing approximately double the number of neighbours than a single atomic domain, can exchange electrons with more partners, so that the superbasin probabilities tend to decrease over those in the single-domain case. Second, it is clear that given the overall formal electroneutrality of the superbasins in all cases the $p(n = Z_A + Z_B)$ is always maximum, and that the larger the overall localization, the larger its value.

It is also clear that the $n \pm 1$ and $n \pm 2$ probabilities decay from the $n = Z_A + Z_B$ maximum very differently in these systems as compared to the ionic cases, with small asymmetries between the plus and minus signs. For instance, the Na-Cl superbasin allows only for ± 1 electron exchanges, much like the Na-Na and Cl-Cl ones, which are characterized by very asymmetric profiles: the Na-Na pair preferentially loses its electron, while the Cl-Cl pair prefers gaining it, as it graphically illustrated in Fig. 1. In both the diamond and graphite superbasins the ± 1 and ± 2 electron exchanges are all relevant, with no major sign asymmetry, which is also clearly appreciable in Fig. 1, in which for both systems, the C atom shows a symmetrical distribution, showing a flexible nature, gaining or loosing electrons with the same probability. This is another sign of the larger spatial extension of covalency in these systems.

Closer inspection reveals that the intra-layer superbasin probabilities in graphite are slightly larger than their equivalent in diamond.

Table 6 Probabilities of selected RSRSs in *bcc* Na. Na′ denotes a nearest neighbour.

n_{Na}	$p^1(n_{\mathrm{Na}})$	n_{Na}	$n_{\mathrm{Na}'}$	$p^1(n_{\mathrm{Na}}) \times p^1(n_{\mathrm{Na}'})$	$p^2(n_{\mathrm{Na}}, n_{\mathrm{Na}'})$	$p^2 - p^1_{\mathrm{Na}} p^1_{\mathrm{Na}'}$
11	0.4159	11	11	0.1730	0.1733	0.0003
10	0.3254	10	11	0.1353	0.1352	-0.0001
12	0.2019	10	10	0.1059	0.0971	-0.0088
13	0.0489	11	12	0.0840	0.0844	0.0004
14	0.0069	10	12	0.0657	0.0712	0.0055
15	0.0006	12	12	0.0408	0.0378	-0.0030
9	0.0003	11	13	0.0203	0.0205	0.0002
16	0.0003	10	13	0.0159	0.0186	0.0027

This result may in principle appear counter-intuitive, since the electrons in graphite are expected to be a more delocalized than in diamond. There is no dissonance, however: whereas electrons in diamond have a short-range strong delocalization in the three spatial directions, graphite displays strong two-dimensional short-range exchanges,[15] plus much smaller longer-ranged metallic-like components. This is already evident from DIs. The graphite $\delta^{1,2}_{\perp} = 0.020$ is of the same order as the nnn $\delta^{1,3} = 0.039$ in diamond. Delocalization of electrons between graphite layers, even if the shortest way is taken, encounter as much a resistance as that for an electron being exchanged with its second neighbours in diamond.

Na *bcc*: the metallic case

The tight association between metallic bonding and long-range electron delocalization has not only been put forward in many instances (see Refs. 45–47 and references therein), but has also already been proven by us.[38,48] With Pauling's words, a metal can be seen as a system with its atoms bonded by a partially covalent tie.[49] The partial covalent character of metallic bonding is quickly confirmed by the DI values in crystalline sodium, larger than in an ionic picture but smaller than that of a pure covalent bond $\delta^{\mathrm{Na,Cl}} < \delta^{\mathrm{Na,Na}} < \delta^{\mathrm{C,C}}$ (see Table 1). Notice that the number of neighbors should also be taken into account. If the total variance of an atom is taken into account with the data in the Table, the above ordering is also unchanged. The partial covalency of the metallic link is also evidenced by the EDFs' distribution tail, wider than that of crystalline NaCl but narrower than the distribution in diamond, as shown in Fig. 1.

Metallic sodium and other simple alkali metals are usually introduced as models of the free-electron

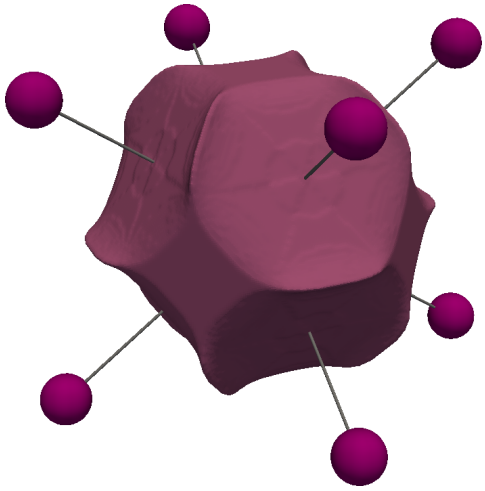

Figure 5 QTAIM basins of the Na *bcc*.

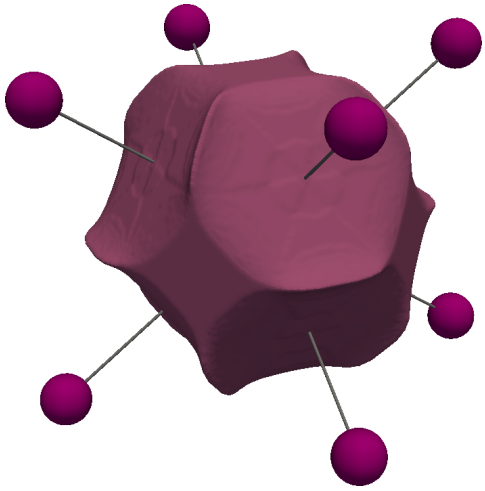

Figure 6 QTAIM basins of the Na *bcc*.

gas. According to it, their valence s electrons in their ground state give rise to a partially filled valence band in which the Fermi level lies, yielding gapless systems in the one-particle approximation. However, it is relevant to keep in mind that in these ground states electron delocalization, although much more long-ranged than in other systems, still decays fast with distance. The inspection of DIs in Na carried out by Baranov and Kohout[15] showed a distant sharing of 0.44 pairs for Na *bcc*, which is notably higher than the 0.02 value obtained for the NaCl crystal, but smaller than the distant sharing observed in diamond (0.74 pairs) and graphite (0.64 pairs). It is even smaller than the 0.66 distant shared pairs in the metallic Cu *fcc* system. However, one must take into account that the Na atom has formally only one valence electron

available for sharing. It is consequently informative to take a look at the fraction of distant pairs being shared, which indicates a distant sharing almost twice as large as that in graphite, diamond and crystalline copper.[15]

Each Na atom has 8 nearest neighbours at a distance of 3.66 Å located along the diagonal of the cubic unit cell, as depicted in Fig. 6, but displays also bond critical points with its 6 second nearest neighbours, 4.22 Å apart. The delocalization to the 8 closest neighbors amounts to $8 \times \delta^{\mathrm{Na,Na}} = 8 \times 0.096 = 0.771$ (see Table 1). Considering additionally the 6 next nearest neighbors (i.e., $6 \times 0.06 = 0.36$) yields the close sharing $\varsigma_{\mathrm{c}}^{\mathrm{Na}} = 1.13$. The sharing with the over-next 8 neighbors in the diagonal direction is much smaller ($8 \times 0.003 = 0.024$). Notice the slow decay of the electron sharing. Actually, we have shown that the DIs decay exponentially with distance in insulators while algebraically in metals.[38,39,48] This is the real space signature of metallic character, and helps to understand why metallic densities do not necessarilly show some peculiar feature when compared other type of bonds.

Table 6 collects a representative set of probabilities from the EDF of crystalline sodium. $p^1(n_{\mathrm{Na}} = 11) = 0.416$, and a rather interesting asymmetry appears with $p^1(n_{\mathrm{Na}} < 10)$ being significatnly under-represented with respect to $p^1(n_{\mathrm{Na}} > 10)$. This has a relatively simple physical origin in the very costly second and further ionization energies of sodium. Given the low ionization energy of sodium, the second highest probability is that corresponding to a Na^+ cation ($n_{\mathrm{Na}} = 10$), whereas $p^1(n_{\mathrm{Na}} = 9)$ for the Na^{2+} cation is seventh in the list, a result of the very high second electron affinity. This means that the physical properties of atoms are thus visible in the shape of EDFs. The joint two-domain distribution shows once more the tendency toward nearest-neighbour electron sharing, and also toward the formation of stabilizing neighbouring ionic pairs. Thus, joint events in which an electron is shared between nearest neighbors, so that $n_{\mathrm{Na}} + n_{\mathrm{Na'}} = 22$, are favoured, as well as those giving rise to oppositely charged neighbours. Notice that both the probability of a double cation as well as a double anion are clearly under-represented with respect to their independent events value. It would certainly be interesting to examine how the probabilities of variable arrangements of cationic and anionic centers vary with distance, since these were used in the early valence-bond ideas of metallic bonding. We expect to do that in the near future.

Conclusions

Electron Distribution Functions (EDFs) provide a real space analog of Pauling resonance structures, and allow for the computation of chemical bonding descriptors based on the fluctuation of electron populations in terms of their cumulant moments. This includes not only the standard two-center delocalization indices, but general n-center bond orders. EDFs provide the probability of finding a given partition of the N electrons of a system when a real space decomposition, like that provided by the QTAIM, is selected. In a sense, they tell us about how likely it is to "observe" a given electron distribution, or electronic snapshot. To each two-center bond order or DI, the EDF assigns a joint two-domain probability distribution, i.e. a rather large set of probabilities. EDFs thus provide a fine-grained description of spatial electron localization and delocalization. A plurality of different bond types may be compatible with a given localization or delocalization index that can be uncovered by analyzing their EDFs. Most importantly, in many cases, the EDF probabilities can be directly related to simple physical and chemical behaviour.

In the present study the EDF machinery has been generalized to extended solids. It has been shown, by examining few archetypal ionic, covalent and metallic examples, that the information stored in the EDF is valuable, justifying with exquisite detail how, to what extent, and how far, electrons localize and delocalize spatially in the solid state. These results are completely compatible with previous knowledge regarding LIs and DIs in the same systems here examined. The width of EDFs is very narrow in ionic systems, getting increasingly wider as they evolve toward covalency. In all cases, from NaCl to metallic sodium, electron sharing is basically found to be a short-range phenomenon occurring between nearest neighbours, although the remaining delocalization tails may decay more or less fast depending on the insulating or metallic character of the systems.

The calculation of EDFs in extended systems may be added to the real space toolkit of orbital invariant quantities with an impact on the understanding of chemical interactions in solids.

Acknowledgements

We thank the Spanish MINECO, grant PGC2018-095953-B-I00 and the European Union FEDER for funding.

References

(1) Lewis, G. N. The atom and the molecule. Journal of the American Chemical Society. **1916**, 38, 762–786.

(2) Pauling, L. The shared-electron chemical bond. Proceedings of the national academy of sciences **1928**, 14, 359–362.

(3) Heitler, W.; London, F. Interaction between neutral atoms and homopolar binding according to quantum mechanics. Zeitung Physik **1927**, 44, 455–472.

(4) Gimarc, B. M. Molecular structure and bonding: the qualitative molecular orbital approach; Academic Press, 1979.

(5) Shaik, S.; Hiberty, P. A chemist's guide to valence bond theory; John Wiley & Sons. Hoboken, N.J., 2008.

(6) Bader, R. F. Atoms in molecules; Wiley Online Library, 1990.

(7) Popelier, P. L.; Brémond, É. A. Geometrically faithful homeomorphisms between the electron density and the bare nuclear potential. International Journal of Quantum Chemistry **2009**, 109, 2542–2553.

(8) Anderson, J. S. M.; Ayers, P. W.; Hernandez, J. I. R. How Ambiguous Is the Local Kinetic Energy? The Journal of Physical Chemistry A **2010**, 114, 8884–8895.

(9) Gillespie, R. Molecular geometry; Van Nostrand Reinhold London, 1972.

(10) Martín Pendás, Á.; Francisco, E.; Blanco, M. Pauling resonant structures in real space through electron number probability distributions. The Journal of Physical Chemistry A **2007**, 111, 1084–1090.

(11) Martín Pendás, Á.; Francisco, E. Quantum Chemical Topology as a Theory of Open Quantum Systems. Journal of Chemical Theory and Computation **2018**, 15, 1079–1088.

(12) Martín Pendás, Á.; Francisco, E. Local spin and open quantum systems: clarifying misconceptions, unifying approaches. Physical Chemistry Chemical Physics **2021**, 23, 8375–8392.

(13) Francisco, E.; Martín Pendás, Á.; Blanco, M. A. EDF: Computing electron number probability distribution functions in real space from molecular wave functions. Computer Physics Communications **2008**, 178, 621–634.

(14) Francisco, E.; Martín Pendás, Á. Electron number distribution functions from molecular wavefunctions. Version 2. Computer Physics Communications **2014**, 185, 2663–2682.

(15) Baranov, A. I.; Kohout, M. Electron localization and delocalization indices for solids. Journal of computational chemistry **2011**, 32, 2064–2076.

(16) Becke, A.; Edgecombe, K. A simple measure of electron localization in atomic and molecular systems. Journal of Chemical Physics **1990**, 92, 5397.

(17) Kohout, M. A measure of electron localizability. Int. J. Quant. Chem. **2004**, 97, 651.

(18) Francisco, E.; Martín Pendás, Á.; Blanco, M. A. Electron number probability distributions for correlated wave functions. Journal of Chemical Physics **2007**, 126, 094102.

(19) Martín Pendás, Á.; Francisco, E.; Blanco, M. Spin resolved electron number distribution functions: How spins couple in real space. The Journal of chemical physics **2007**, 127, 144103.

(20) Francisco, E.; Casals-Sainz, J. L.; Rocha-Rinza, T.; Martín Pendás, A. Partitioning the DFT exchange-correlation energy in line with the interacting quantum atoms approach. Theoretical Chemistry Accounts **2016**, 135, 1–8.

(21) Martín Pendás, Á.; Francisco, E. Chemical Bonding from the Statistics of the Electron Distribution. ChemPhysChem **2019**, 20, 2722–2741.

(22) Martín Pendás, Á.; Francisco, E.; Blanco, M. An electron number distribution view of chemical bonds in real space. Physical Chemistry Chemical Physics **2007**, 9, 1087–1092.

(23) Bader, R.; Stephens, M. Fluctuation and correlation of electrons in molecular systems. Chemical Physics Letters **1974**, 26, 445–449.

(24) Bader, R. F.; Stephens, M. E. Spatial localization of the electronic pair and number distributions in molecules. Journal of the American Chemical Society **1975**, 97, 7391–7399.

(25) Mayer, I. Charge, bond order and valence in the ab initio SCF theory. Chemical Physics Letters **1983**, 97, 270–274.

(26) Wiberg, K. B. Application of the pople-santry-segal CNDO method to the cyclopropylcarbinyl and cyclobutyl cation and to bicyclobutane. Tetrahedron **1968**, 24, 1083–1096.

(27) de-la Roza, A. O.; Martín Pendás, Á.; Johnson, E. R. Quantitative Electron Delocalization in Solids from Maximally Localized Wannier Functions. Journal of Chemical Theory and Computation **2018**, 14, 4699–4710.

(28) La Penna, G.; Tiana, D.; Giannozzi, P. Measuring Shared Electrons in Extended Molecular Systems: Covalent Bonds from Plane-Wave Representation of Wave Function. Molecules **2021**, 26, 4044.

(29) Elk 2.2.10. http://elk.sourceforge.net, 2013.

(30) Perdew, J. P.; Wang, Y. Accurate and simple analytic representation of the electron-gas correlation energy. Physical Review B **1992**, 45, 13244.

(31) Kohout, M. DGrid. version 5.2,www2.cpfs.mpg.de/∼kohout/Documents/dgrid-html/dgrid.html, Dresden, 2021.

(32) Blum, V.; Gehrke, R.; Hanke, F.; Havu, P.; Havu, V.; Ren, X.; Reuter, K.; Scheffler, M. Ab initio molecular simulations with numeric atom-centered orbitals. Computer Physics Communications **2009**, 180, 2175–2196.

(33) Fradera, X.; Austen, M.; Bader, R. The Lewis model and beyond. The Journal of Physical Chemistry A **1999**, 103, 304–314.

(34) Martín Pendás, Á.; Francisco, E.; Blanco, M. An electron number distribution view of chemical bonds in real space. Physical Chemistry Chemical Physics **2007**, 9, 1087–1092.

(35) Martín Pendás, Á.; Costales, A.; Luaña, V. Ions in crystals: The topology of the electron density in ionic materials. I. Fundamentals. Physical Review B **1997**, 55, 4275–4284.

(36) Luaña, V.; Costales, A.; Martín Pendás, A. Ions in crystals: The topology of the electron density in ionic materials.II. The cubic alkali halide perovskites. Physical Review B **1997**, 55, 4285–4297.

(37) Martín Pendás, Á.; Costales, A.; Luaña, V. Ions in Crystals: The Topology of the Electron Density in Ionic Materials. III. Geometry and Ionic Radii. The Journal of Physical Chemistry B **1998**, 102, 6937–6948.

(38) Gallo-Bueno, A.; Francisco, E.; Martín Pendás, Á. Decay rate of real space delocalization measures: a comparison between analytical and test systems. Physical Chemistry Chemical Physics **2016**, 18, 11772–11780.

(39) Gallo-Bueno, A.; Kohout, M.; Martín Pendás, Á. Decay rate of correlated real-space delocalization measures: Insights into chemical bonding and mott transitions from hydrogen chains. Journal of chemical theory and computation **2016**, 12, 3053–3062.

(40) Angyan, J.; Loos, M.; Mayer, I. Covalent bond orders and atomic valence indices in the topological theory of atoms in molecules. The Journal of Physical Chemistry **1994**, 98, 5244–5248.

(41) Matito, E.; Poater, J.; Solà, M.; Duran, M.; Salvador, P. Comparison of the AIM delocalization index and the mayer and fuzzy atom bond orders. The Journal of Physical Chemistry A **2005**, 109, 9904–9910.

(42) Matito, E.; Solà, M.; Salvador, P.; Duran, M. Electron sharing indexes at the correlated level. Application to aromaticity calculations. Faraday discussions **2007**, 135, 325–345.

(43) Feixas, F.; Matito, E.; Poater, J.; Solà, M. On the performance of some aromaticity indices: A critical assessment using a test set. Journal of computational chemistry **2008**, 29, 1543–1554.

(44) Martín Pendás, Á.; Francisco, E.; Blanco, M. Charge transfer, chemical potentials, and the nature of functional groups: answers from quantum chemical topology. Faraday discussions **2007**, 135, 423–438.

(45) Baranov, A. I.; Ponec, R.; Kohout, M. Domain-averaged Fermi-hole analysis for solids. The Journal of chemical physics **2012**, 137, 214109.

(46) Macchi, P.; Sironi, A. Chemical bonding in transition metal carbonyl clusters: complementary analysis of theoretical and experimental electron densities. Coordination chemistry reviews **2003**, 238, 383–412.

(47) Silvi, B.; Gatti, C. Direct space representation of the metallic bond. The Journal of Physical Chemistry A **2000**, 104, 947–953.

(48) Martín Pendás, Á.; Guevara-Vela, J. M.; Crespo, D. M.; Costales, A.; Francisco, E. An unexpected bridge between chemical bonding indicators and electrical conductivity through the localization tensor. Physical Chemistry Chemical Physics **2017**, 19, 1790–1797.

(49) Pauling, L. The Nature of the Chemical Bond; Cornell Univ. Press.: Ithaca, N. Y., third Ed., 1960.